Metal centers in biomolecular solid-state NMR

José Pedro Silva,[1,2] Linda Cerofolini,[1] Stefano Giuntini,[1,3] Vito Calderone,[1,3] Carlos F. G. C. Geraldes,[4] Anjos L. Macedo,[2] Giacomo Parigi,[1,3] Marco Fragai,[1,3] Enrico Ravera,[1,3] Claudio Luchinat[1,3,*]

1. Magnetic Resonance Center (CERM), University of Florence and Consorzio Interuniversitario Risonanze Magnetiche di Metalloproteine, Via L. Sacconi 6, 50019 Sesto Fiorentino (FI), Italy

2. UCIBIO-Requimte, Faculty of Sciences and Technology, Universidade NOVA de Lisboa, Caparica, Portugal

3. Department of Chemistry "Ugo Schiff", University of Florence, Via della Lastruccia 3, 50019 Sesto Fiorentino (FI), Italy

4. Department of Life Sciences and Coimbra Chemistry Center, University of Coimbra, Coimbra, Portugal

Corresponding Author:

Prof. Claudio Luchinat

CERM, University of Florence

Via Sacconi 6, 50019 Sesto Fiorentino, Italy

Tel +39 055 4574296

FAX +39 055 4574253

Email: claudioluchinat@cerm.unifi.it

Keywords:

Electronic structure, biosolids, paramagnetic NMR, sensitivity, resolution

Highlights:

1. The electronic structure of paramagnetic centers has a strong impact on the solid-state NMR spectra of the biomolecules to which they are bound.

2. Slowly relaxing electron spins are usually associated to fast relaxation of the nuclear resonances and to small shifts, therefore are most useful for obtaining distance restraints in the form of paramagnetic relaxation enhancements.

3. Fast relaxing electron spins usually feature an anisotropic magnetic susceptibility that is reflected in large pseudocontact shifts, which in turn can be used to achieve unambiguous structural information.

4. Large pseudocontact shifts can yield sizeable intermolecular contributions in crystals, and may contain sufficient information to fully reconstruct the supramolecular arrangement of protein crystals.

5. Contact shifts are strongly dependent on the reciprocal arrangement of the nuclei with respect to the metal center. Different conformations observed in a crystal could be reflected in largely different contact shift values.

Abstract: Solid state NMR (SSNMR) has earned a substantial success in the characterization of paramagnetic systems over the last decades. Nowadays, the resolution and sensitivity of solid state NMR in biological molecules has improved significantly and these advancements can be translated into the study of paramagnetic biomolecules. However, the electronic properties of different metal centers affect the quality of their SSNMR spectra differently, and not all systems turn out to be equally easy to approach by this technique. In this review we will try to give an overview of the properties of different paramagnetic centers and how they can be used to increase the chances of experimental success.

Introduction

In parallel to the development of biomolecular NMR, there has been a flourishing literature about NMR of paramagnetic biomolecules: many proteins inherently bind metal ions, which are either paramagnetic, or that can be substituted for a paramagnetic analogue, and most of the systems that do not naturally bind metals can be functionalized with metal binding tags.

With the methodological and technical improvements that have brought solid-state NMR sensitivity and resolution to compare with that of solution NMR, there is reason to question whether the paramagnetic effects that are observed in solution are maintained in the solid state. The answer to this question is non-trivial because it depends on a number of effects that are related to the way the electron-nucleus interactions is modulated in solution and in solids [1,2].

The presence of a static magnetic field induces magnetic dipole moments within an object, which result in a macroscopic magnetization, and the larger the applied field the larger the magnetization, with a proportionality constant known as magnetic susceptibility [3]. Some objects are *diamagnetic*, meaning that they are weakly repelled by the magnetic field. On the contrary, *paramagnetic* objects tend to be sizeably attracted by the field. The reason of the different behavior is that electrons in closed shells create currents that tend to counteract the static magnetic field, whereas unpaired electrons tend to align at least partly with the field, generating a contribution to the magnetic susceptibility that opposes and overcomes the diamagnetic one. If the unpaired electron(s) can occupy a set of degenerate orbitals, which are related by rotation about an axis (and the set of orbitals does not result half-filled), electron motion generates orbital angular momentum. The orbital momentum gives anisotropy to the magnetic susceptibility.

The unpaired electron in stable organic radicals, such as a nitroxides or trityls, sits in orbitals that can be seen as mainly arising from p-type atomic orbitals, which have a small orbital momentum that

becomes smaller when the p-character of the molecular orbitals (MO) is decreased. When unpaired electrons belong to a d-block metal, the situation is more complicated. Free ions would have a large angular momentum, but d-block metals tend to exist as complexes, and the ligand field removes the degeneracy of the five d orbitals, quenching the orbital angular momentum. However, in perfectly O_h or T_d symmetry, the t_{2g} orbitals and the e_g orbitals remain degenerate among themselves, and if these orbitals are not half-filled, the orbital momentum is not completely quenched and yields a sizeable anisotropy; finally admixing with low lying states in lower symmetry environments also dequenches the orbital momentum. In all those cases, spin-orbit coupling (SOC) can be significant, due to the much larger nuclear charge of transition metals w.r.t. carbon and nitrogen; for systems with more than one unpaired electron, SOC gives rise to zero-field splitting, amplifying the effect due to the angular component, with the result that the magnetic susceptibility is even more anisotropic [4–6]. As is for an experimentally observable, anisotropic quantity, magnetic susceptibility is described by a rank-2 symmetric tensor.

The electronic structure of the metal center also strongly impacts the electron relaxation times. The topic is treated in detail in references [7,8]. The electron relaxation time largely depends on the availability of low-lying excited states. In S=1/2 systems, in the presence of low-lying excited states, Orbach and Raman processes may be effective, allowing for the electron spin transitions during transitions between lattice vibrational levels (in the Orbach mechanism, two phonons with a difference in energy equal to the Zeeman energy provide the energy for jumps from the ground to the excited state and viceversa, in the Raman mechanism two phonons with a difference in energy equal to the Zeeman energy simultaneously interact allowing for a change of the electron spin state). When the energy jumps between ground and excited states are much larger than the vibrational energies, other mechanisms, like spin-rotation, stochastic fluctuation of the g-tensor and/or of the hyperfine coupling tensor between unpaired electron and metal nucleus, can be important. In S>1/2 system, with excited states far in energy from the ground state, electron relaxation is determined by

modulation of transient ZFS, i.e. of the component of the ZFS with zero average, arising from the instantaneous deformations of the coordination sphere of the metal. When excited states are close in energy to the ground state (as in nearly doubly or triply degenerate ground state, arising in the presence of distortions of the idealized symmetry) Orbach processes can also be efficient.

A "rule of the thumb" can be devised that is: the absence of low-lying excited states which causes limited anisotropy of the magnetic susceptibility also causes inefficient electron relaxation (which translates into very efficient nuclear relaxation).[7]

Table 1. Metal ions with their electron configuration and the total spin quantum number, together with the usual electron relaxation values and axial magnetic susceptibility anisotropies.

Metal	Electronic configuration	S	Electron relaxation time (s)	Axial magnetic susceptibility anisotropies (10^{-32} m^3, absolute values)
Mn^{2+}	d^5	5/2	$\approx 10^{-8}$ (field dependent, may reach 10^{-10})	<0.1
Fe^{3+} (H.S.)	d^5	5/2	10^{-9}–10^{-10} (field dependent, may reach 10^{-11})	0.5
Fe^{3+} (L.S.)	d^5	1/2	10^{-11}–10^{-13}	3
Fe^{2+} (H.S.)	d^6, 5–6 coord.	2	10^{-12}–10^{-13}	2.5
	d^6, 4 coord.	2	$\approx 10^{-11}$	2

Co^{2+} (H.S.)	d^7, 5–6 coord.	3/2	5×10^{-12}–10^{-13}	7
	d^7, 4 coord.	3/2	$\approx 10^{-11}$	3
Co^{2+} (L.S.)	d^7	1/2	10^{-9}–10^{-10}	1
Ni^{2+}	d^8, 5–6 coord.	1	$\approx 10^{-10}$ (strong field dependence)	2
	d^8, 4 coord.	1	$\approx 10^{-12}$	1
Cu^{2+}	d^9	1/2	$(1–5) \times 10^{-9}$	0.5
Gd^{3+}	f^7	7/2	10^{-8}–10^{-9} (field dependent, may reach below 10^{-10})	0.2
Ln^{3+}	f^1-f^6,f^8-f^{13}		10^{-12}-10^{-13}	0.1-50

A nucleus sitting at a certain distance from the metal center perceives the presence of the metal center with a certain magnetic susceptibility, which changes the value of the magnetic field that the nucleus is sensing, and does so to different extent (and sign) for different orientations of the nucleus-metal vector with respect to the static magnetic field. A different value of field translates into a different chemical shift value. However, if the magnetic susceptibility is isotropic, as it happens for instance in complexes with ^6S or ^8S ground state that have quenched orbital momentum, the rotational average of the different shift values coincides with the chemical shift that the nucleus would have in the diamagnetic analogue. Based on this reasoning, the paramagnetic center appears innocent. Now it is important to recall that if, during the time of the acquisition of the NMR spectrum, the molecule is not allowed to reorient, then all the different chemical shift values would appear at the same time. This is the case of powders or frozen solutions. If the magnetic susceptibility is anisotropic, then the rotational average of the shifts corresponding to different orientations does not coincide anymore

with the shift in the diamagnetic compound. The difference is referred to as *pseudocontact shift* (PCS).

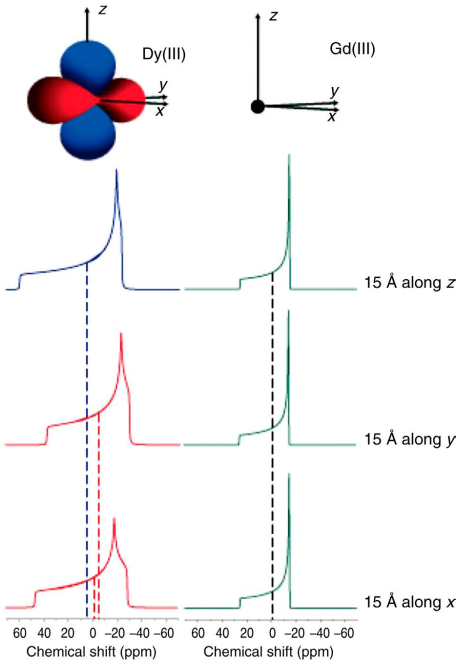

Figure 1. Powder patterns of dipolar shielding anisotropy on nuclei located at 15 Å distance from the metal center, in the case of Dy(III) and Gd(III). The magnitude of the magnetic susceptibility is calculated with equation 2.29 from reference [7], the magnetic susceptibility anisotropy of Dy is simulated on the basis of the experimentally determined PCS values from ref. [9], and the powder patterns are calculated with Simpson [10,11], using the zcw28656 crystal file, available from http://nmr.au.dk/downloads/. Reproduced with permission from reference [12].

The unpaired electron is, in general, not localized on a single point (the metal center) but rather extends to MOs that can reach several bonds away from the metal. Incidentally, we note that nuclei that are close to the metal center, but do not have unpaired electron density directly delocalized on them (see below), sense the unpaired spin as a distribution rather than as a point dipole.[13] Treatments to describe this situation range from breaking up the unpaired electron density on the ligand nuclei [14–19] to integration over the ab-initio calculated unpaired electron density [20,21].

Finally, in every point in space where the MO with the unpaired electron has a nonzero value, the average electron magnetic moment sensed by the nucleus is different from zero and is proportional to the fraction of unpaired electron density present at that point. Furthermore electrons that are paired in MOs sense the unpaired electron and the one that has the same sign of the unpaired electron spin density will have a slight preference to occupy the region of space of its MO which is closer to the unpaired electron itself, whereas the other will tend to stay farther (spin polarization, see figure 2). These two mechanisms account for the effect that is called *Fermi contact shift*. The sum of contact and pseudocontact shifts is the paramagnetic shift, also called "hyperfine shift" [7].

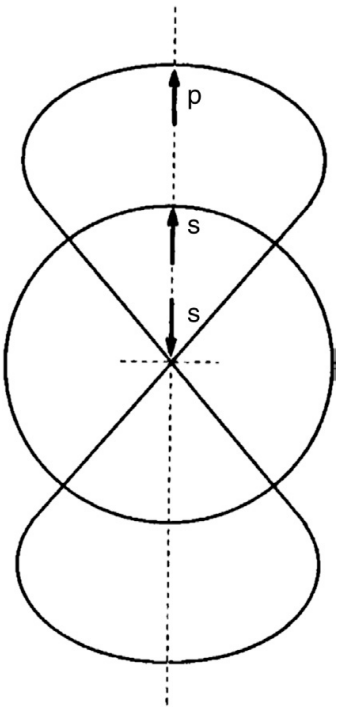

Figure 2. The unpaired electron in a 2p orbital affects the distribution of the two paired electrons in the 1s orbital. Reproduced with permission from reference [7].

The difference between liquids and solids, as these two states are seen by NMR, is that in liquids stochastic molecular reorientation occurs, whereas in solids it is abolished. While this may seem trivial, it has profound consequences on relaxation: a molecule in solution reorients and an

NMR-active nucleus in this molecule randomly samples different values of (e.g.) chemical shift. This yields a modulation of its interaction energy that causes relaxation. In a solid the same molecule does not tumble, thus each nucleus experiences a single chemical shift value etc. Only the interactions whose Hamiltonian does not commute with itself at any moment of time, such as multinucleus dipole-dipole interaction remain incoherently modulated also in the solid state. The following table (reproduced with permission from [22]) presents the nuclear interactions and how they contribute to relaxation in solids or liquids.

Table 2. Nuclear interactions and their outcome in liquids and in solids in terms of relaxation. Adapted with permission from reference [22].

Interaction	Liquids	Solids
Heteronuclear dipole-dipole coupling	Incoherently modulated by reorientation (τ_R).	Coherently modulated by MAS and heteronuclear decoupling. [23–26]
Homonuclear dipole-dipole coupling	Incoherently modulated by reorientation (τ_R).[27]	Induces sizable broadening because of zero-energy spin flip-flops.[28]
Chemical Shielding Anisotropy	Incoherently modulated by reorientation (τ_R).[29]	Coherently averaged by MAS.[30]
Quadrupolar coupling	Incoherently modulated by reorientation (τ_R).	Reduced by MAS due to the symmetry of the quadrupolar Hamiltonian.
Electron-nucleus dipole-dipole coupling.	Incoherently modulated by the fastest between reorientation	Incoherently modulated by the fastest between electron relaxation (τ_e) and exchange

	(τ_R), electron relaxation (τ_e) and exchange (τ_M).[31–33,7]	(τ_M), in case exchange can occur.[34,2,7]
Curie-spin interaction (see below for a detailed discussion)	Incoherently modulated by the fastest among reorientation (τ_R) and exchange (τ_M).[35,36,4,7]	Coherently modulated by MAS.[37] May be reintroduced by chemical exchange.[12]

In solid state NMR, the same principle for PCSs measurement as in solution is applied after the magic angle spinning (MAS) averaging of the dipolar shielding, allowing the NMR resonance to be centered at the new isotropically averaged position [38–43]. In solution, PCSs are determined only by the paramagnetic species within the molecule, whereas in crystals the PCSs arise from the contributions from all paramagnetic species close to the observed nucleus (intramolecular [44]), as well as from those present in neighbor molecules (intermolecular). In the case where the paramagnetic metal ion is in the periphery of the protein, the nuclei of neighbor molecules, closer to the metal ion, may experience a intermolecular effect larger than the intramolecular one [19,40,45–47]. Both contributions contain exploitable information. The intramolecular contributions are analogous to the PCSs obtained in solution, and therefore can be used for molecular structure determination. As for the intermolecular contributions, these contain information regarding the relative orientations of the biomolecules in the crystalline structure and consequentially can be used to determine the crystal lattice. These two contributions can be isolated by labeling strategies [45,48,49], however at a cost of lower resolution and/or signal-to-noise ratio. Further precautions should be taken because distinctive spatial compositions of the paramagnetic and diamagnetic neighbors generate multiple sets of PCSs. This effect was simulated and represented in Fig. 3 with the increase in concentration (0.7%, 20%, 40%, 50%, 60%, 70% 80%, 90%, 100%) of the paramagnetic molecules in the crystal lattice [12].

A)

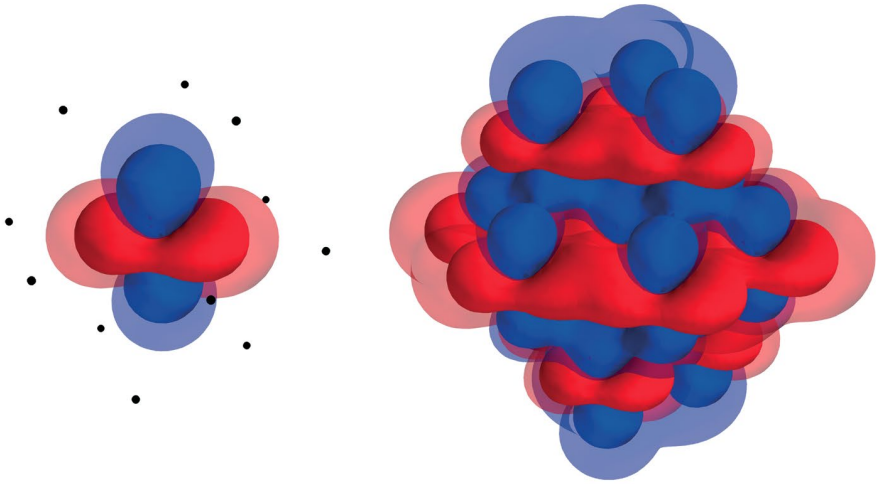

B)

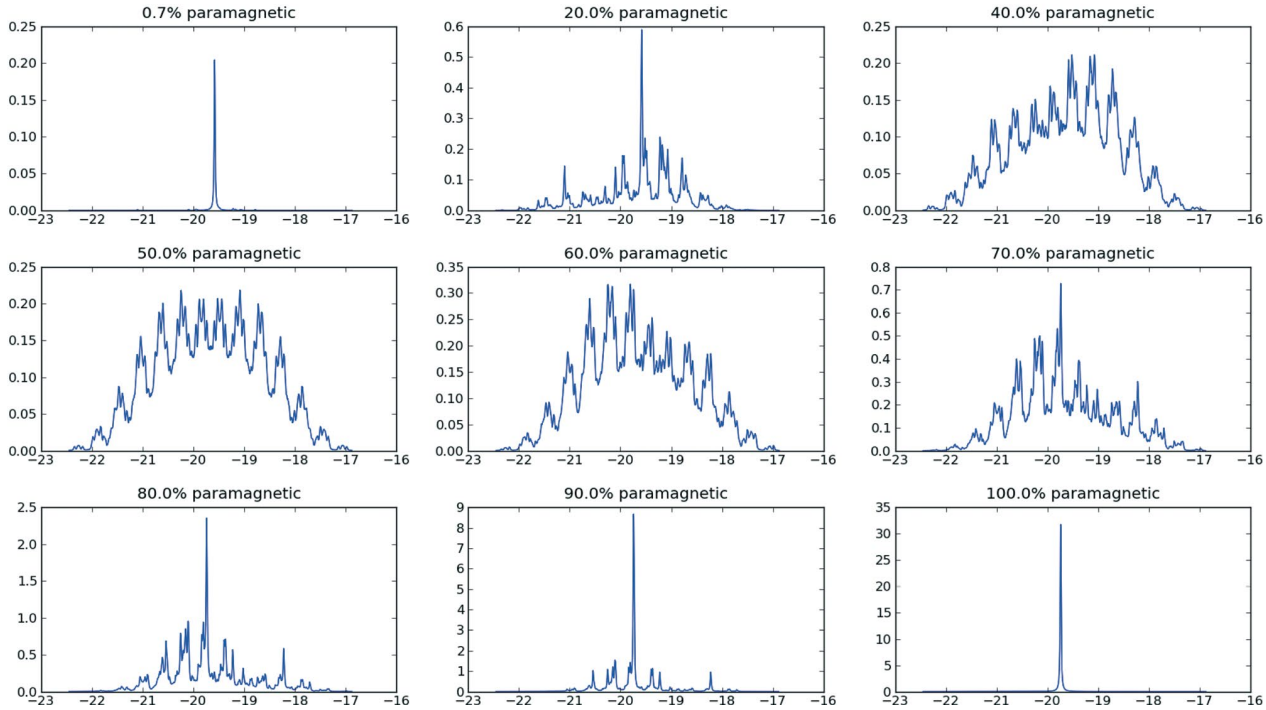

Figure 3. Simulation of the effect of different levels of paramagnetic metal occupancy for a hexagonal compact lattice where each metal ion (black dots) is separated by 40 Å from each nearest neighbor. A) Isosurfaces of the pseudocontact shift for the isolated tensor (left) and for the 13 sites of the simulated crystal lattice, corresponding to the extreme cases of infinite dilution and 100% occupancy; B) appearance of a single pseudocontact-shifted peak for a nucleus at 20 Å from the

intramolecular metal ion, with increasing paramagnetic metal occupancy. The x axis shows the chemical shift (in ppm). Note that the intensity scale (y axis) is changed in every frame to allow visualization and that the intensity increases dramatically when 100% occupancy is approached. Reproduced with permission from reference [12].

With the introduction of a paramagnetic center in a molecule (for the moment leaving the distinction between solids and liquids) other effects should be taken into consideration, such as the increased relaxation rate of nuclei close to the unpaired electron spin(s). This increased effect in the nuclear relaxation rates is called paramagnetic relaxation enhancement (PRE) [7]. The PREs depend on how the electron-nucleus dipole-dipole interaction is modulated: one source of modulation is the electron relaxation because, as the electron flips, the nucleus finds itself cycling between configurations that are separated in energy by twice the value of the dipolar energy [27,31] (Solomon-Bloembergen); another source of modulation is the fact that during stochastic reorientation of the molecule, as it happens in solution, the nucleus experiences a different shift due to the magnetic susceptibility of the metal center (see figure 1) [35,36] (Curie-spin relaxation). This second effect is larger the larger the magnetic susceptibility. The effect on the low field R_1 and on R_2 is more important as the electron relaxation time gets longer, as in paramagnetic radicals and in metal ions like copper(II), manganese(II), high spin iron(III), gadolinium(III), oxovanadium(IV). At high fields and in slowly reorienting systems Curie-spin relaxation can become relevant, in particular for those metals having a large magnetic anisotropy (which is usually linked with a short electron lifetime) [7,50]. Given that stochastic reorientation is abolished in solids, each nucleus senses a distribution of shielding values that is static and hence cannot cause relaxation, thus Curie-spin relaxation should be absent [37]. However, intramolecular motions can modulate the orientation and magnitude of the magnetic anisotropy [51], especially for lanthanoids, for which the 4f-orbitals containing the unpaired electrons, which tend not to participate into the bonding, have energies/orientations that are strongly impacted by the coordination. It is speculated that this behavior is the source of the sizeable line broadening encountered in some cases in lanthanoid-containing protein crystals [12].

The case of iron

Heme-containing proteins were probably the first paramagnetic biological system studied by solid-state NMR.[52] Iron(III) in heme can be either low-spin (S=1/2) or high-spin (S=5/2), depending on the strength of the ligand field. For low spin, the ground state is degenerate, which causes a relatively rapid electron relaxation and a significant dequenching of the orbital magnetic moment, from which an anisotropic magnetic susceptibility arises. Therefore the spectra tend to feature rather narrow lines and measurable pseudocontact shifts. For the high spin, the ground state is non degenerate and there are no low-lying excited levels with the same multiplicity, therefore electron relaxation is rather slow (10^{-11} to 10^{-9} s), which causes severe line broadening, and SOC is only active at the second order, which yields in a small anisotropy. The first studies by the McDermott group therefore focused on the use of deuterium to mitigate the line broadening, to observe solid-state NMR signals also in the vicinity of the heme moiety, even for spin states where solution NMR signals are too broad or undetectable [53]. Solomon relaxation depends on the square of the gyromagnetic ratio, which for deuterium is 0.15 with respect to the proton, therefore the expected paramagnetic relaxation is about 2% relative to proton. This ensures that solid-state spectra have sufficient resolution and sensitivity. The spinning sidebands for deuterium MAS reflect two interactions, the deuterium quadrupolar coupling and the interaction with the unpaired electron(s) (Figure 4). In addition, the fact that the paramagnetic shielding is so anisotropic translates into a Curie-spin contribution to the relaxation of the same nucleus in solution which is comparable to (but likely larger than) the Solomon contribution.

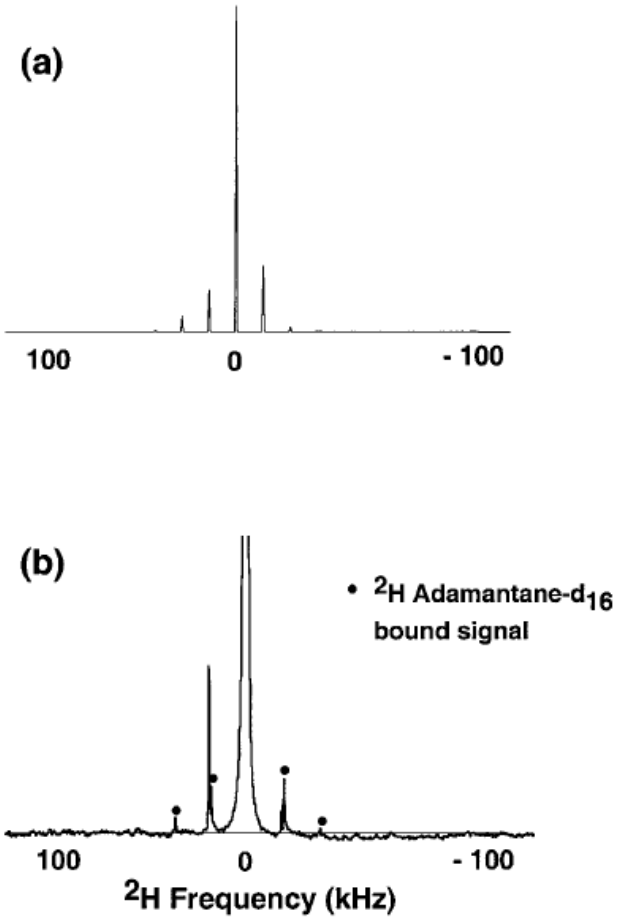

Figure 4. ^{2}H spectra (A - simulation, B -experimental) of adamantane bound to cytochrome P450 camphor 5-exo-hydroxylase (high-spin, S=5/2). The simulation assumes no quadrupolar coupling and 6.5 kHz of dipolar interaction, reflecting a rapid motion of the ligand within the active site of the protein [54].

Furthermore, the exploitation of PREs and PCSs, complemented by selective labeling strategies, permitted to identify the ligand positions, and to characterize the binding mode of ligands to cytochrome P450, resulting in conformation changes [55]. More recently, the structural topology of the membrane bound cytochrome P450 was obtained by solid-state NMR [42], allowing for the building of a model of the membrane-bound complex between cytochrome b_5 and cytochrome P450 by the combined use of solution and solid-state NMR [56]. The solid state data, acquired for the bicelle-bound system at room temperature, also show that the backbone structure of the

transmembrane domain of cytochrome b_5 is not significantly altered by the interaction with cytochrome P450, whereas the mobility of cytochrome b_5 is considerably reduced [41].

Solid state NMR spectra can show narrow linewidths and high sensitivity also for very large membrane protein complexes, like the uniformly ^{13}C,^{15}N-labeled cytochrome bo_3 ubiquinol oxidase (144 kDa) [57]. The spectra can be a source of site-specific information, with chemical details relevant to understand protein function, including the protonation states of residues, side-chain conformation and information about dynamics.

The case of copper: relaxation as a source of structural information and paramagnetism-assisted condensed data collection

Among the first examples of high-resolution solid-state NMR characterization of paramagnetic proteins there are copper(II)-containing systems. Copper(II) is a d^9 ion, thus has a non-degenerate ground state. The single unpaired electron is mostly relaxed through the Raman mechanism, yielding electron relaxation times of the order of a few nanoseconds. In turn, this translates into a significant broadening of the nuclear resonances. The spin orbit coupling admixes the ground state with the excited states (lying at about 13000 cm^{-1}) yielding a modest dequenching of the orbital magnetic moment that causes some anisotropy in the g-values and in the magnetic susceptibility.

Superoxide dismutase 1 is a metalloenzyme that catalyzes the conversion of superoxide to dioxygen and peroxide. In its natural form it carries a copper and a zinc ion in the active site ((Cu,Zn)-SOD1). During the catalytic cycle the copper ion cycles between oxidation states +1 and +2. This protein was the first for which a complete assignment of the resonances was achieved via solid-state NMR. The spectra of (Cu,Zn)-SOD1 are nicely resolved, both in ^{13}C-detection of the fully protonated protein and in ^{1}H-detection of the deuterated protein (Figure 5) [58,59]. The presence of the copper(II)

ion sizably impacts on the linewidth of some signals (Figure 5D,E), and it was also demonstrated that the reduction of the longitudinal relaxation time could be translated into structural information. There are several examples in the literature describing the usefulness of PRE in structural studies, including microcrystalline preparations [60,61,34], membrane proteins [62], and even for the characterization of copper(II) binding to beta-amyloid fibrils [63].

The augmented relaxation introduced by the presence of copper ions or other slow-relaxing metal centers (manganese(II) and gadolinium(III)), can be exploited by increasing the experiment repetition rate, thus boosting sensitivity. For the specific case of heteronuclear detection, this advantage can be taken further by fast spinning the sample because the requirements for heteronuclear decoupling diminish and consequently the power deposited on the sample and on the coil decreases [64], therefore a long interscan delay is not needed to avoid damage to the instrument and to the sample. This strategy can be successfully applied to different sample systems, including microcrystalline proteins [65,66], membrane proteins [67,68] and protein aggregates [69].

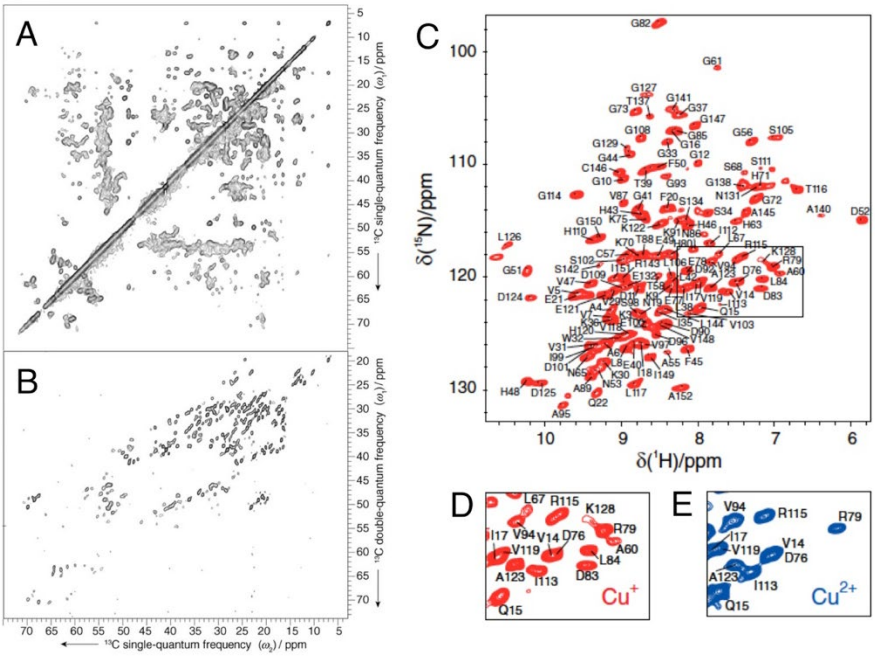

Figure 5. A) ^{13}C-^{13}C-DARR and B) ^{13}C-^{13}C refocused INADEQUATE recorded on oxidized (Cu,Zn)-SOD1, reproduced with permission from reference [58]. C) ^{1}H-^{15}N correlation spectrum recorded on reduced (Cu,Zn)-SOD1; a close-up of a selected region of the spectrum for the reduced (D) and oxidized (E) protein are shown, reproduced with permission from reference [59].

The case of cobalt: obtainment of structural restraints

With the evolution of solid-state NMR and the increased understanding of the paramagnetic effects in solids, the first structure of a paramagnetic protein appeared. This paramagnetic protein was the catalytic domain of the matrix metalloproteinase 12, where the natural zinc(II) ion was substituted by a high-spin cobalt(II) ion. High spin cobalt(II) in a pseudooctahedral coordination has a large magnetic susceptibility anisotropy and fast electron relaxation [7,70]. It is important to recall that fast electron relaxation for (e.g.) high spin pseudooctahedral cobalt(II), causes less broadening as opposed to the slow relaxation of (e.g.) copper(II). These properties make it possible to obtain resolved spectra. Figure 6 shows a NCA spectrum of Co(II)-substituted catalytic domain of MMP12.

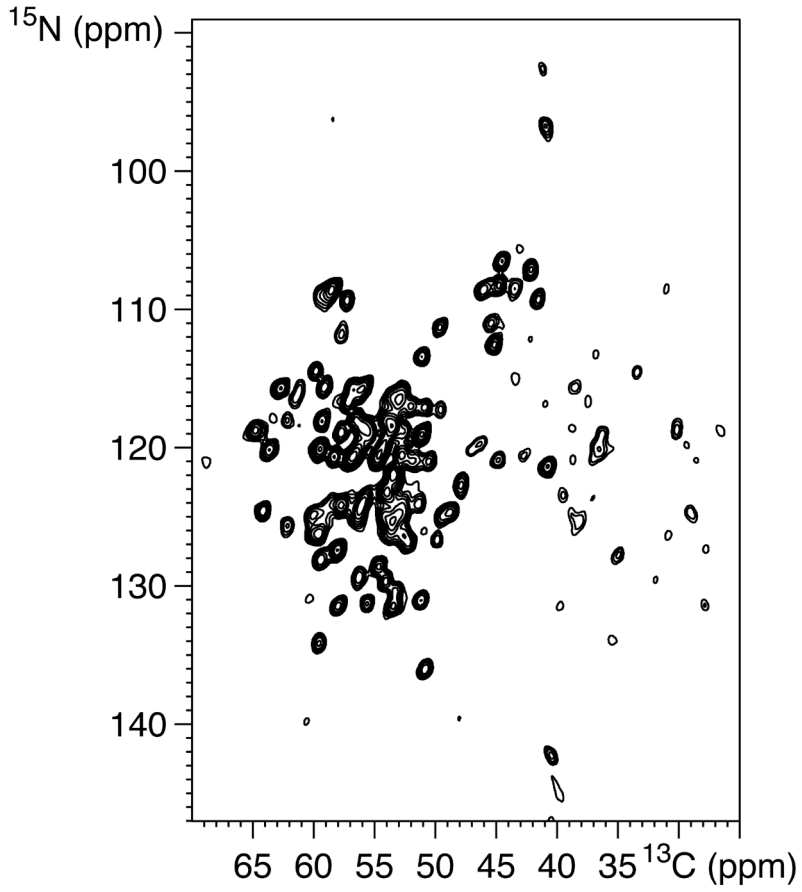

Figure 6: N-CA correlation spectrum acquired on the cobalt(II)-substituted catalytic domain of MMP12. Spectra were acquired at 270 K, 11.5 kHz MAS, 75 kHz ^{1}H decoupling [71].

The high quality of the NMR data allowed for the determination of the structure of this enzyme. In particular, the unambiguous information provided by PCSs was capital to achieve the assignment of ambiguous carbon-carbon distance information [45]. Through the preparation of paramagnetically-diluted samples, it was possible to dissect the intermolecular and the intramolecular contribution [45], until enough data were obtained for the determination of the structure [72]. Later, the PCSs obtained for the non-diluted crystals were analyzed including crystal mate molecules and this procedure allowed to determine simultaneously the structure and the crystal packing from PCS data, only including the lattice constants available from X-ray diffraction spectra [47].

The favorable electronic properties of this system, combined with fast magic angle spinning, made it also possible to observe the signals of the residues that coordinate the metal center with high resolution [73] (Fig. 7).

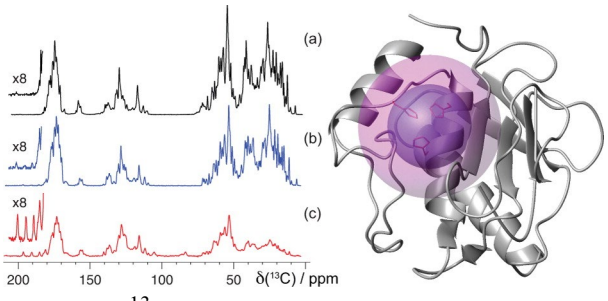

Figure 7. (a–c) ^{13}C NMR spectra of microcrystalline CoMMP-12 recorded (a) at 22 kHz MAS at 20 T (10k scans, 3 s interscan delay, total time = 15 h) and (b, c) at 60 kHz MAS at 21.2 T (15k scans, 2 s and 0.2 s interscan delay, respectively, total times = 15 h and 3h). (d) Regions of CoMMP-12 inaccessible by solid-state NMR at 22 kHz (outer sphere) and at 60 kHz (inner sphere). Reprinted with permission from reference [73].

It is also possible to replace a cobalt(II) ion in the position of the zinc ion in the active site of superoxide dismutase. This replacement yields sizeable pseudocontact shifts [59], which could be combined with the PRE measured for the copper(II) sample (see above) to obtain a structure with higher accuracy [73].

The case of Fe_4S_4

Another example of highly favorable electronic properties is the oxidized state of the high-potential iron-sulfur protein from Halorhodospira Halophila (hereon Halophila I HiPIP). This protein contains a Fe_4S_4 cubane cluster, which can exist in a reduced state behaving as a S=0 system and in an oxidized state behaving as a S=1/2. Nominally, in the oxidized state three irons are in the +3 oxidation state, and one is in the +2 oxidation state. The interplay between their magnetic properties can be represented as the coupling between two pairs, where each pair is defined as the net result of two opposing interactions, namely, of superexchange, via the bridging sulfides, favoring antiparallel coupling of individual ion spins,[74] and of double-exchange, associated with electron delocalization over the pair, favoring parallel spin coupling.[75–77] In this situation, the "ferric" couple has spin 4 and is forced by the mixed pair, formally comprising of two $Fe^{2.5+}$, thus having spin 9/2, in an

antiparallel spin configuration. The exchange coupling in the Fe_4S_4 cubane cluster warrants rather short electron relaxation times and the S=1/2 spin state does not yield sizable PCSs. Therefore, high quality solid state spectra were obtained (Fig. 8) [78,79], even for a fully protonated sample. Also in this case the good resolution arises from the disruption of the dipolar network caused by hyperfine shift and paramagnetic relaxation enhancement [73].

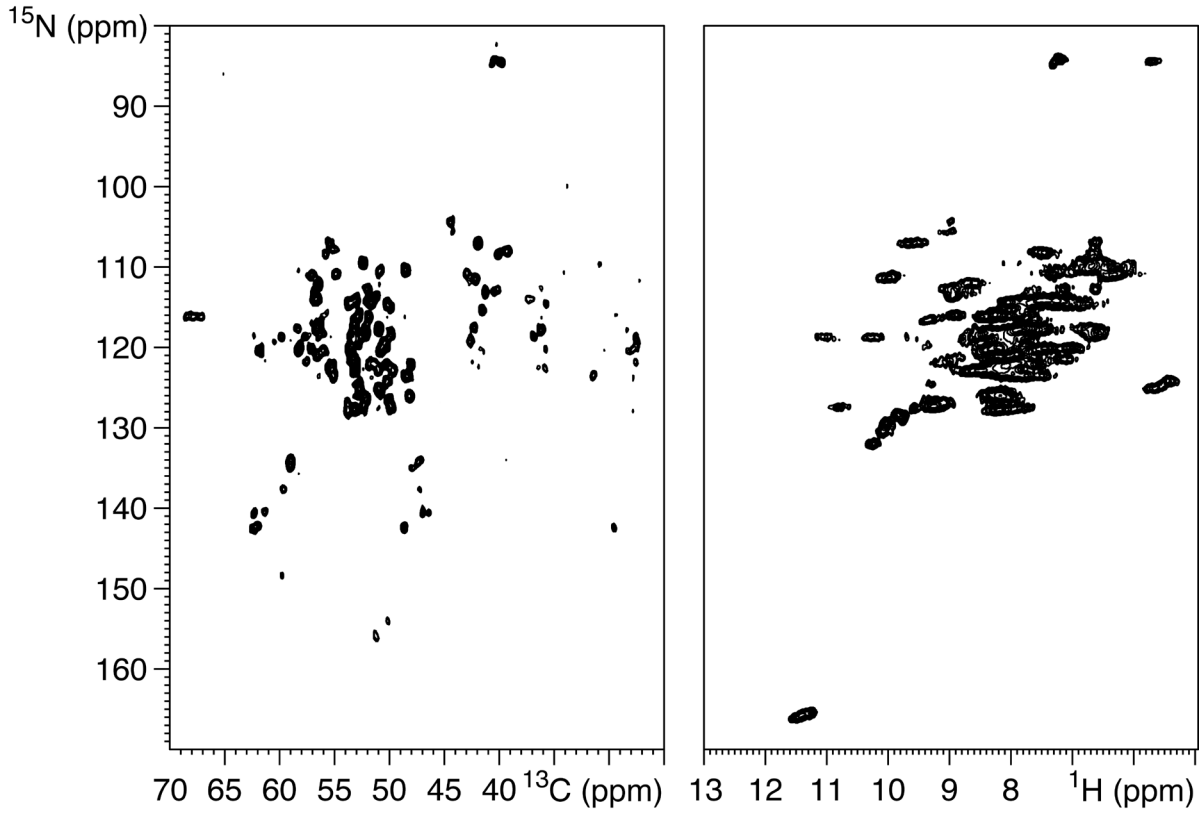

Figure 8. N-CA[80] and H-N[60,81] correlation spectra acquired on the oxidized Halophila I HiPIP. Spectra were acquired at 235 K at stator outlet, 60 kHz MAS, 12.5 kHz ^{1}H decoupling. Reproduced with permission from reference [78].

In the crystals, there are two molecules in the asymmetric unit, and those molecules differ, among the other things, for the dihedral angles intervening between the cysteine methylene protons and the metal center. Fast magic angle spinning also allows for the observation of far shifted resonances, which correspond to the methylene protons of the cysteine residues that coordinate the

cubane cluster, in particular, around 100 ppm for ^{1}H (see Figure 9) and 400 ppm for ^{13}C spectra [79]. These are the most shifted values ever measured by solid-state NMR for metalloproteins. In addition, the ^{1}H-detected SSNMR spectrum, shown in Figure 9, captures the distinct signatures from the two conformations of the protein present in the asymmetric unit of the crystal, featuring an overall backbone RMSD of 0.67 Å. Interestingly enough, assuming that the interconversion between two forms exists in solution, it is possible to explain the higher-than-expected slope of Cys50Hb2 and Cys 33 Hb1 that were observed in the original report.

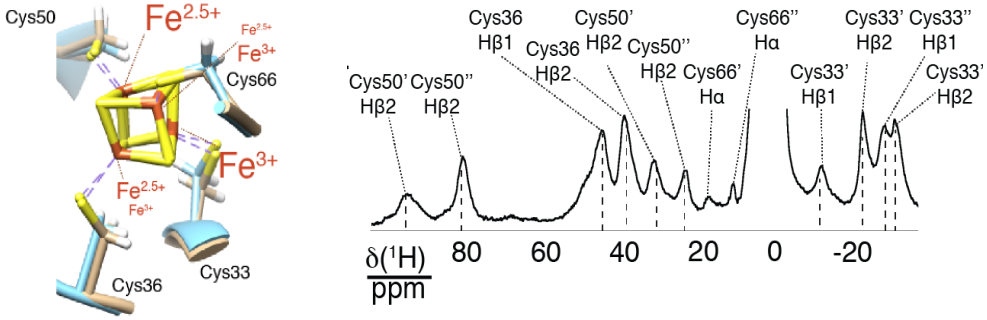

Figure 9: Superposition of the Fe_4S_4 cluster and the coordinating cysteines in the two molecules present in the asymmetric unit of EhHiPIP I and ^{1}H double-adiabatic echo [82] spectrum. (‘) and (“) denote the two different forms observed for that residue, corresponding to the two molecules. *Adapted with permission from* [79]. *Copyright 2017 American Chemical Society.*

The case of nickel: the first observation

In the literature there are several examples describing the use of nickel and its paramagnetic properties in biomolecules, such as: human Carbonic Anhydrase II (hCAII) [70,83–85], rubredoxin [86], thioredoxin [87] and azurin. However, the case of nickel(II)-containing proteins in the solid state was so far unexplored. Here we provide a preview of an ongoing work showing that spectra of high quality can be obtained in the solid state also for nickel(II) containing proteins, through the example of hCAII (Figs. 10-11). HCAII naturally contains a diamagnetic zinc ion its active site. However, zinc can be

substituted by several metal ions (e.g.: vanadyl(IV), manganese(II), iron(II), cobalt(II), nickel(II), copper(II) and cadmium(II)) [83]. Nickel(II) has a d^8 configuration, thus it has potentially two unpaired electrons, yielding S=1. In solution it was determined that this nickel (II) can be five-coordinated and six coordinated, with a square pyramidal geometry or pseudo-octahedral geometry, respectively. When nickel(II) has any of these two coordination geometries, the ground state is singly degenerate and the energy separation between the ground and excited states is large, therefore an electron relaxation rate close to 100 ps and a very small $\Delta\chi$ is expected and observed [7,70]. Therefore, observation of signals from nuclei close to the metal center should not be taken for granted.

However, our data indicate that also the presence of nickel(II) can induce hyperfine shifts that contribute to breaking the proton dipolar bath, and this contributes to yield high resolution spectra, even without the deuteration of the protein (Fig. 11). Nickel(II) can induce rather large contact shifts, due to the covalent character of its bonding to the nitrogen ligands, which justifies the presence of ^{1}H resonances that shift to the 50-80 ppm region (Fig. 12). These protons from the histidines (H94, H96 and H119) that are coordinating the Ni(II) ion at the active center correspond to the protons of the imidazole ring in the meta-like position relative to the metal-binding nitrogen atom.

In the X-ray structure of the same crystal form the nickel ion in the active site is observed in two different coordination geometries: octahedral and pentacoordinate, with either three or two water molecules coordinating the metal center (in preparation). Interestingly, at variance with the case of the HIPIP, the two different environments do not appear to be reflected in a doubling of the contact-shifted resonances, suggesting that they may be interconverting rapidly on the NMR timescale. Based on previous literature[85] (although the values in reference 72 refer to possibly larger rearrangements of the coordination environment) differences of the order of 10 ppm in the contact shift could be expected, which implies an interconversion frequency larger than 8 kHz. A close inspection of the NCA and NCO spectra also does not seem to show a detectable doubling of the resonances, although

the PCSs are expected to be in the range -1 to 0.5 ppm (i.e.: larger than the linewidth of the ^{13}C resonances), and a systematic comparison with the zinc(II) analogue crystals is ongoing.

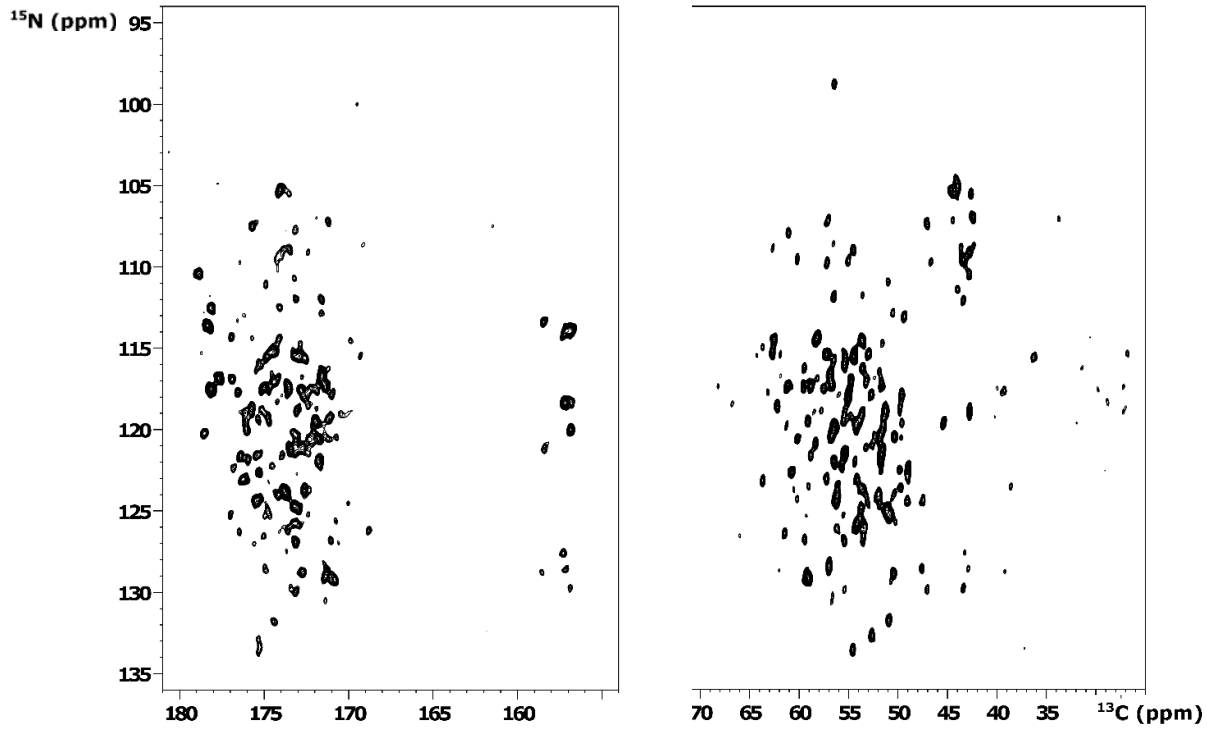

Figure 10. N-CO and N-CA correlation spectra acquired on hCAII-Ni. The spectra were acquired at 800 MHz, 260 K at stator outlet, 14 kHz MAS.

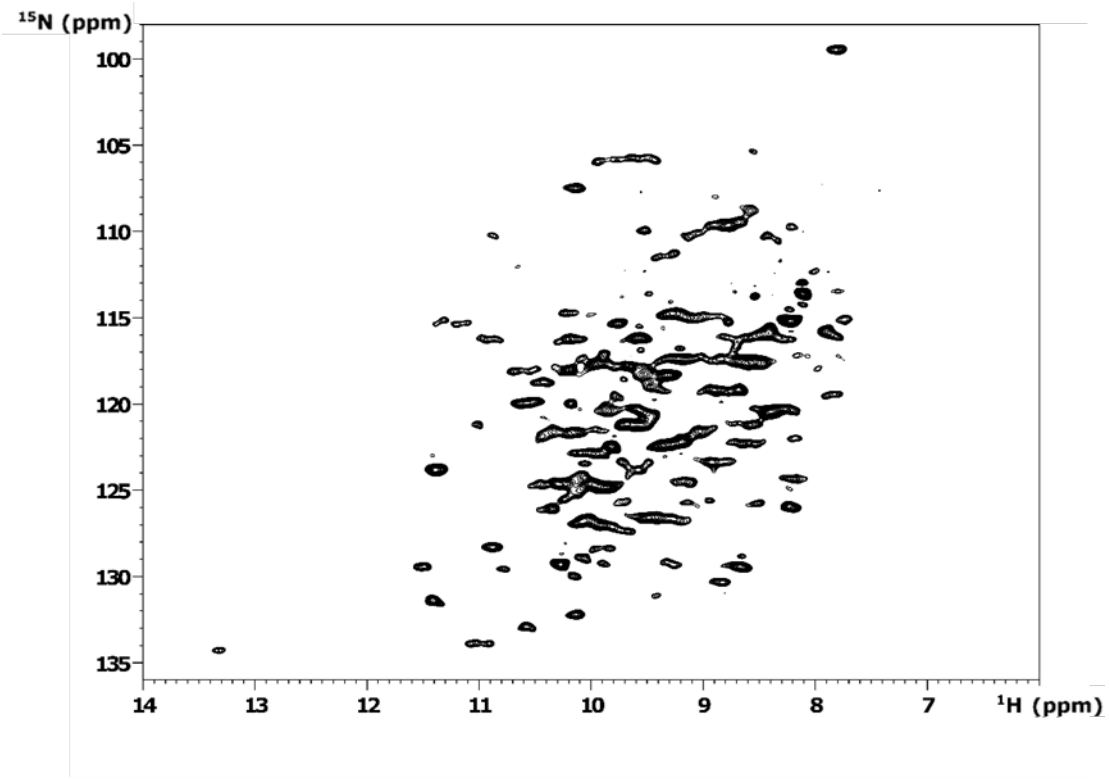

Figure 11. HN correlation spectrum acquired on hCAII-Ni. Spectrum was acquired at 800 MHz, 248 K at stator outlet, 65 KHz MAS.

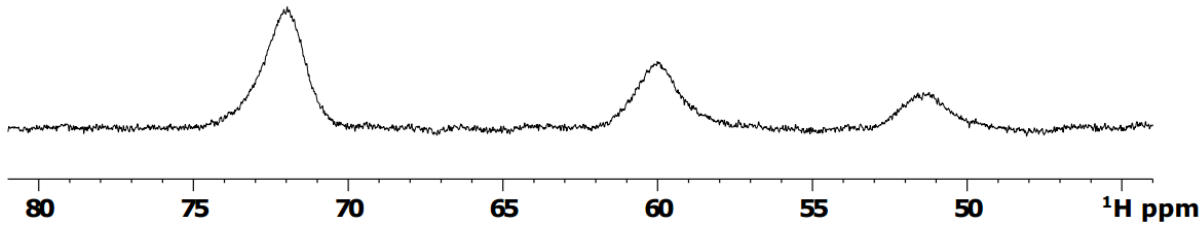

Figure 12. Enlargement of the low-field region of the ^{1}H NMR spectrum of hCAII-Ni. The spectrum was acquired at 800 MHz, 248 K at stator outlet, 65 KHz MAS.

The puzzle of lanthanoids

Up to now we have considered how the electronic properties of transition metal ions and their clusters translate into the appearance of the NMR spectra. Another well studied source of paramagnetism is the lanthanoid ions. In solution NMR these ions are increasingly being used to extract structural information that arises from the large anisotropy of their magnetic susceptibility

[88]. For SSNMR, the major application of lanthanoids is the characterization of small complexes and materials.[40,89] Up to date there is only one example of the use of a lanthanoid-tagged protein to obtain highly resolved spectra [90], which were obtained using a dipicolinic acid tag, structurally related to the complexes analyzed in references [37,40]. In general, however, obtaining well resolved SSNMR spectra with paramagnetic lanthanoids is a challenge due to several factors. These factors can be incomplete binding of the lanthanoid-tag to the target protein and small fluctuations in the lanthanoid's sphere of coordination. An incomplete binding of the lanthanoid-tag generates a heterogeneous crystal lattice with bound and unbound tag. This diverse metal occupancy generates different chemical environments in the neighboring molecules leading to a significant heterogeneous resonance shift (as already discussed and exemplified in Fig. 3B) of the detected nucleus [12]. A more subtle and less controllable effect is related to the fact that even small fluctuations in the lanthanoid's first coordination sphere, even as small as the rotation of a single water molecule [51], may strongly modulate the magnetic susceptibility tensor. Such a behavior is typical of lanthanoids, and relates to the fact that the 4f orbitals, which bear the unpaired electron(s), are more internal and do not participate in the binding (with the possible exception of ytterbium(III) with softer ligands such as cyclopentadienyl [91]). In turn, this makes the 4f orbitals susceptible of larger changes upon minor perturbation of the ligand field than what happens, for instance, for 3d metals, where a change in the coordination geometry (e.g. trigonal bipyramid to square pyramid [92]) must occur to cause a sizeable variation of the magnetic susceptibility tensor. An illuminating example along these lines is offered by the case of lanthanoid-DOTA complexes. The molecule has overall a four-fold symmetry, which is broken by the presence of the water ligand, hydrogen bonded to the carboxylic arms, which yields a two-fold symmetry. The two-fold symmetry causes the magnetic susceptibility to be rhombic, with the main axis directed in the plane, but the reorientation of the water and the establishment of a different hydrogen bonding network can turn the axis around by 90°. Therefore, the interconversion between the two states would result in an axial magnetic susceptibility, with the main axis now

directed along the metal-water bond, and an overall reversal of the sign of the anisotropy. Therefore, the interconversion among different conformations modulates the magnetic susceptibility as sensed by the nuclei, and this is expected to reintroduce a Curie-spin-like relaxation and consequently cause a line broadening, which is more severe the larger the variation of the magnetic susceptibility [12].

Materials and methods

The nickel(II) derivative of hCAII was obtained from the zinc(II)-loaded enzyme by a demetallation/metallation approach. hCAII was expressed and purified as previously reported [70]. For the demetallation of hCAII-Zn, a solution with the final concentration of 200 mM sodium phosphate, 50 mM pyridine-2,6-dicarboxylic acid (PDA), pH 7, was added to the protein solution and incubated overnight at 277 K [93]. After demetallation, the apo-hCAII was buffer exchanged to 10 mM HEPES, pH 6.8, using 10,000 MWCO Amicon centrifugation devices.

The paramagnetic hCAII-Ni was prepared by monitoring the titration of the apo enzyme with a nickel(II) sulfate solution with 2D ^{1}H-^{15}N HSQC solution NMR spectra, acquired on a 500 MHz spectrometer equipped with triple-resonance cryo-probe.

Crystals were obtained by the sitting drop vapor diffusion method at 293 K by mixing an equal volume of the sample (58.5 mg/mL of protein in 10 mM HEPES, pH 6.8) and of a solution containing 100 mM HEPES pH 7.5, 2.9 M ammonium sulfate.

SSNMR experiments were performed on the crystalline preparation of hCAII-Ni in 1.3 and 3.2 mm rotors. All the spectra were recorded on a Bruker Avance III HD 800 MHz spectrometer (19 T, 201.2 MHz ^{13}C Larmor frequency), equipped with 3.2 and 1.3 mm MAS probe heads in triple-resonance mode.

The inter-scan delay was set to 2.5 and 1 s in ^{13}C-detected and ^{1}H-detected experiments, respectively. The temperature at the stator outlet was set to 260 K and 248 K in ^{13}C-detected and ^{1}H-detected experiments, respectively.

Standard ^{13}C-detected SSNMR spectra were acquired at MAS frequency of 14 kHz using the pulse sequences reported in the literature [94]. The nonselective 90° pulses were set to 2.5 µs at 100 kHz RF-field amplitude (^{1}H), 4.6 µs (54 kHz RF-field amplitude (^{15}N), and 4 µs at 62.5 kHz RF-field amplitude (^{13}C). Proton decoupling was applied at 100 kHz with a SW_f-TPPM sequence [95].

Standard ^{1}H-detected 1D ^{1}H and 2D ^{1}H-^{15}N CP HSQC SSNMR spectra were acquired at MAS frequency of 65 kHz using the pulse sequences reported in the literature [59,81]. The ^{1}H spectral window for 1D ^{1}H was set to 195 ppm. The nonselective 90° pulses were 1.65 µs (^{1}H) and 4 µs (^{15}N). Proton decoupling was applied at 17 kHz with a SW_f-TPPM sequence [96].

All the spectra were processed with the Bruker TopSpin 3.2 software and analyzed with the program CARA.

Conclusions

Nowadays, one of the biggest challenges in biological solid-state NMR is the obtainment of high resolution spectra. Sample preparation represents a critical point in these regards [97,98], but this is not a sufficient condition for achieving high resolution in the case of paramagnetic molecules. However, the knowledge of the electronic structure of the metal centers may allow one to predict the behavior of different systems and, if possible, to choose the most appropriate metal ion for studying a given system. When the metal is chosen appropriately, the presence of paramagnetic species is beneficial for the success of SSNMR experiments, not only when paramagnetic probes are added in solution for increasing the relaxation rates and thus recycling faster, but also in protein

structural studies thanks to the onset of effects, like PCSs and PREs, which provide additional structural restraints without molecular weight-dependent line broadening.

Acknowledgements

This work has been supported by Fondazione Cassa di Risparmio di Firenze, the European Commission (contract #675858). The authors acknowledge the use of resources of Instruct-ERIC, an ESFRI Landmark, supported by national member subscriptions. J.P.S. acknowledges FCT for the doctoral fellowship PD/BD/135180/2017 integrated in the PhD Program in NMR applied to chemistry, materials and biosciences.

[1] M.J. Knight, I.C. Felli, R. Pierattelli, L. Emsley, G. Pintacuda, Magic Angle Spinning NMR of Paramagnetic Proteins, Acc. Chem. Res. 46 (2013) 2108–2116. doi:10.1021/ar300349y.

[2] C.P. Jaroniec, Structural studies of proteins by paramagnetic solid-state NMR spectroscopy, J. Magn. Reson. 253 (2015) 50–59. doi:10.1016/j.jmr.2014.12.017.

[3] B.I. Bleaney, B. Bleaney, Electricity and magnetism, Oxford University Press, Oxford, 1976.

[4] I. Bertini, C. Luchinat, G. Parigi, Magnetic susceptibility in paramagnetic NMR, Prog. Nucl. Magn. Reson. Spectrosc. 40 (2002) 249–273.

[5] G. Pintacuda, A.Y. Park, M.A. Keniry, N.E. Dixon, G. Otting, Lanthanide labeling offers fast NMR approach to 3D structure determinations of protein-protein complexes, J. Am. Chem. Soc. 128 (2006) 3696–3702. doi:10.1021/ja057008z.

[6] J. Koehler, J. Meiler, Expanding the utility of NMR restraints with paramagnetic compounds: Background and practical aspects, Prog. Nucl. Magn. Reson. Spectrosc. 59 (2011) 360–389. doi:10.1016/j.pnmrs.2011.05.001.

[7] I. Bertini, C. Luchinat, G. Parigi, E. Ravera, NMR of paramagnetic molecules: applications to metallobiomolecules and models, 2017.

[8] L. Banci, I. Bertini, C. Luchinat, Nuclear and electron relaxation. The magnetic nucleus-unpaired electron coupling in solution, VCH, Weinheim, 1991.

[9] I. Bertini, M.B.L. Janik, Y.-M. Lee, C. Luchinat, A. Rosato, Magnetic Susceptibility Tensor Anisotropies for a Lanthanide Ion Series in a Fixed Protein Matrix, J. Am. Chem. Soc. 123 (2001) 4181–4188.

[10] M. Bak, J.T. Rasmussen, N.C. Nielsen, SIMPSON: A General Simulation Program for Solid-State NMR Spectroscopy, J. Magn. Reson. 147 (2000) 296–330.

[11] Z. Tošner, R. Andersen, B. Stevensson, M. Edén, N.C. Nielsen, T. Vosegaard, Computer-intensive simulation of solid-state NMR experiments using SIMPSON, J. Magn. Reson. 246 (2014) 79–93. doi:10.1016/j.jmr.2014.07.002.

[12] A. Bhaumik, C. Luchinat, G. Parigi, E. Ravera, M. Rinaldelli, NMR crystallography on paramagnetic systems: solved and open issues, CrystEngComm. 15 (2013) 8639–8656. doi:10.1039/C3CE41485J.

[13] R.M. Golding, L.C. Stubbs, NMR shifts in paramagnetic systems: a nonmultipole expansion method, J.Magn.Reson. 33 (1979) 627–627.

[14] A.D. Buckingham, P.J. Stiles, Mol.Phys. 24 (1972) 99.

[15] P.J. Stiles, Magnetic octopole contributions to the 'pseudo-contact' chemical shift, Mol. Phys. 27 (1974) 501–509. doi:10.1080/00268977400100451.

[16] P.J. Stiles, On the theory of nuclear shielding by magnetically anisotropic molecules and functional groups, Mol. Phys. 29 (1975) 1271–1276. doi:10.1080/00268977500101071.

[17] R.M. Golding, R.O. Pascual, L.C. Stubbs, On the theory of the pseudocontact contribution to the NMR shifts in paramagnetic systems, Mol.Phys. 31 (1976) 1933.

[18] J.P. Riley, W.T. Raynes, Application of multiple SCF perturbation theory to the tensors which describe the magnetic shielding and the multipole magnetizabilities of molecules, Mol. Phys. 33 (1977) 619–629. doi:10.1080/00268977700100571.

[19] B.J. Walder, K.K. Dey, M.C. Davis, J.H. Baltisberger, P.J. Grandinetti, Two-dimensional NMR measurement and point dipole model prediction of paramagnetic shift tensors in solids, J. Chem. Phys. 142 (2015) 014201. doi:10.1063/1.4904548.

[20] G.T.P. Charnock, I. Kuprov, A partial differential equation for pseudocontact shift, Phys. Chem. Chem. Phys. 16 (2014) 20184–20189. doi:10.1039/C4CP03106G.

[21] E. A. Suturina, I. Kuprov, Pseudocontact shifts from mobile spin labels, Phys. Chem. Chem. Phys. 18 (2016) 26412–26422. doi:10.1039/C6CP05437D.

[22] E. Ravera, The bigger they are, the harder they fall: A topical review on sedimented solutes for solid-state NMR, Concepts Magn. Reson. Part A. 43 (2014) 209–227. doi:10.1002/cmr.a.21318.

[23] U. Haeberlen, J.S. Waugh, Coherent Averaging Effects in Magnetic Resonance, Phys. Rev. 175 (1968) 453–467. doi:10.1103/PhysRev.175.453.

[24] U. Haeberlen, J.S. Waugh, Spin-Lattice Relaxation in Periodically Perturbed Systems, Phys. Rev. 185 (1969) 420–429. doi:10.1103/PhysRev.185.420.

[25] M.M. Maricq, J.S. Waugh, NMR in rotating solids, J. Chem. Phys. 70 (1979) 3300–3316. doi:10.1063/1.437915.

[26] W.P. Rothwell, J.S. Waugh, Transverse relaxation of dipolar coupled spin systems under rf irradiation: Detecting motions in solids, J. Chem. Phys. 74 (1981) 2721–2732. doi:10.1063/1.441433.

[27] I. Solomon, Relaxation Processes in a System of Two Spins, Phys. Rev. 99 (1955) 559–565. doi:10.1103/PhysRev.99.559.

[28] M.J. Duer, Solid-State NMR Spectroscopy Principles and Applications, Blackwell Science, 2002.

[29] J. Cavanagh, W.J. Fairbrother, A.G.I.I.I. Palmer, M. Rance, N.J. Skelton, Protein NMR Spectroscopy. Principles and practice, Academic Press, SanDiego, 2007.

[30] M. Alla, E. Lippmaa, Resolution Limits in Magic-Angle Rotation NMR Spectra of Polycrystalline Solids, Chem.Phys.Lett. 87 (1982) 30–33.

[31] N. Bloembergen, Proton relaxation times in paramagnetic solutions, J.Chem.Phys. 27 (1957) 572–573.

[32] N. Bloembergen, L.O. Morgan, Proton Relaxation Times in Paramagnetic Solutions. Effects of Electron Spin Relaxation, J. Chem. Phys. 34 (1957) 842–850. doi:10.1063/1.1731684.

[33] S.H. Koenig, A Novel Derivation of the Solomon-Bloembergen-Morgen Equations: Application to Solvent Relaxation by Mn(II)-Protein Complexes, J.Magn.Reson. 31 (1978) 1–10.

[34] I. Sengupta, P.S. Nadaud, C.P. Jaroniec, Protein Structure Determination with Paramagnetic Solid-State NMR Spectroscopy, Acc. Chem. Res. 46 (2013) 2117–2126. doi:10.1021/ar300360q.

[35] A.J. Vega, D. Fiat, Nuclear relaxation processes of paramagnetic complexes The slow-motion case, Mol. Phys. 31 (1976) 347–355. doi:10.1080/00268977600100261.

[36] M. Gueron, Nuclear relaxation in macromolecules by paramagnetic ions: a novel mechanism, J.Magn.Reson. 19 (1975) 58–66.

[37] G. Kervern, S. Steuernagel, F. Engelke, G. Pintacuda, L. Emsley, Absence of Curie relaxation in paramagnetic solids yields long ^1H coherence lifetimes, J. Am. Chem. Soc. 129 (2007) 14118–14119.

[38] R.. Wittebort, Selective excitation and quadrupole connectivities in deuterium NMR of paramagnetic solids, J. Magn. Reson. 1969. 83 (1989) 626–629. doi:10.1016/0022-2364(89)90357-0.

[39] H. Lee, T. Polenova, R.H. Beer, A.E. McDermott, Lineshape Fitting of Deuterium Magic Angle Spinning Spectra of Paramagnetic Compounds in Slow and Fast Limit Motion Regimes, J. Am. Chem. Soc. 121 (1999) 6884–6894. doi:10.1021/ja990636u.

[40] G. Kervern, A. D'Aléo, L. Toupet, O. Maury, L. Emsley, G. Pintacuda, Crystal-Structure Determination of Powdered Paramagnetic Lanthanide Complexes by Proton NMR Spectroscopy, AngewChem IntEd Engl. 48 (2009) 3082–3086.

[41] K. Yamamoto, U.H.N. Dürr, J. Xu, S.-C. Im, L. Waskell, A. Ramamoorthy, Dynamic Interaction Between Membrane-Bound Full-Length Cytochrome P450 and Cytochrome b5 Observed by Solid-State NMR Spectroscopy, Sci. Rep. 3 (2013). doi:10.1038/srep02538.

[42] K. Yamamoto, M. Gildenberg, S. Ahuja, S.-C. Im, P. Pearcy, L. Waskell, A. Ramamoorthy, Probing the Transmembrane Structure and Topology of Microsomal Cytochrome-P450 by Solid-State NMR on Temperature-Resistant Bicelles, Sci. Rep. 3 (2013). doi:10.1038/srep02556.

[43] H. Heise, F.H. Köhler, X. Xie, Solid-State NMR Spectroscopy of Paramagnetic Metallocenes, J. Magn. Reson. 150 (2001) 198–206. doi:10.1006/jmre.2001.2343.

[44] S. Balayssac, I. Bertini, M. Lelli, C. Luchinat, M. Maletta, K.J. Yeo, Paramagnetic ions provide precious structural restraints in solid-state NMR of proteins, J. Am. Chem. Soc. 129 (2007) 2218–2219.

[45] S. Balayssac, I. Bertini, A. Bhaumik, M. Lelli, C. Luchinat, Paramagnetic shifts in solid-state NMR of proteins to elicit strucutral information., Proc.Natl.Acad.Sci.USA. 105 (2008) 17284–17289.

[46] I. Bertini, C. Luchinat, G. Parigi, Moving the frontiers in solution solid state bioNMR. A celebration of Harry Gray's 75th birthday, Coord.Chem.Rev. 255 (2011) 649–663.

[47] C. Luchinat, G. Parigi, E. Ravera, M. Rinaldelli, Solid state NMR crystallography through paramagnetic restraints, J. Am. Chem. Soc. 134 (2012) 5006–5009.

[48] I. Bertini, A. Bhaumik, G. De Paepe, R.G. Griffin, M. Lelli, J.R. Lewandowski, C. Luchinat, High-Resolution Solid-State NMR Structure of a 17.6 kDa Protein, J. Am. Chem. Soc. 132 (2010) 1032–1040.

[49] J. Li, K.B. Pilla, Q. Li, Z. Zhang, X. Su, T. Huber, J. Yang, Magic Angle Spinning NMR Structure Determination of Proteins from Pseudocontact Shifts, J. Am. Chem. Soc. 135 (2013) 8294–8303. doi:10.1021/ja4021149.

[50] I. Bertini, C. Luchinat, G. Parigi, R. Pierattelli, NMR of paramagnetic metalloproteins, ChemBioChem. 6 (2005) 1536–1549.

[51] G. Cucinotta, M. Perfetti, J. Luzon, M. Etienne, P.-E. Car, A. Caneschi, G. Calvez, K. Bernot, R. Sessoli, Magnetic Anisotropy in a Dysprosium/DOTA Single-Molecule Magnet: Beyond Simple Magneto-Structural Correlations, Angew. Chem. Int. Ed. 51 (2012) 1606–1610. doi:10.1002/anie.201107453.

[52] A. McDermott, T. Polenova, Solid state NMR: new tools for insight into enzyme function, Curr. Opin. Struct. Biol. 17 (2007) 617–622. doi:10.1016/j.sbi.2007.10.001.

[53] K. Liu, J. Williams, H. Lee, M.M. Fitzgerald, G.M. Jensen, D.B. Goodin, A.E. McDermott, Solid-State Deuterium NMR of Imidazole Ligands in Cytochrome *c* Peroxidase, J. Am. Chem. Soc. 120 (1998) 10199–10202. doi:10.1021/ja9732385.

[54] H. Lee, P.R. Ortiz de Montellano, A.E. McDermott, Deuterium Magic Angle Spinning Studies of Substrates Bound to Cytochrome P450 †, Biochemistry. 38 (1999) 10808–10813. doi:10.1021/bi990463l.

[55] T. Jovanovic, A. McDermott, Observation of ligand binding to cytochrome P450 BM-3 by means of solid-state NMR spectroscopy, J. Am. Chem. Soc. 127 (2005) 13816–13821.

[56] S. Ahuja, N. Jahr, S.-C. Im, S. Vivekanandan, N. Popovych, S.V. Le Clair, R. Huang, R. Soong, J. Xu, K. Yamamoto, R.P. Nanga, A. Bridges, L. Waskell, A. Ramamoorthy, A Model of the Membrane-bound Cytochrome b_5 -Cytochrome P450 Complex from NMR and Mutagenesis Data, J. Biol. Chem. 288 (2013) 22080–22095. doi:10.1074/jbc.M112.448225.

[57] H.L. Frericks, D.H. Zhou, L.L. Yap, R.B. Gennis, C.M. Rienstra, Magic-angle spinning solid-state NMR of a 144 kDa membrane protein complex: E. coli cytochrome bo3 oxidase, J. Biomol. NMR. 36 (2006) 55–71. doi:10.1007/s10858-006-9070-5.

[58] G. Pintacuda, N. Giraud, R. Pierattelli, A. Böckmann, I. Bertini, L. Emsley, Solid-State NMR Spectroscopy of a Paramagnetic Protein: Assignment and Study of Human Dimeric Oxidized CuII–ZnII Superoxide Dismutase (SOD), Angew. Chem. Int. Ed. 46 (2007) 1079–1082. doi:10.1002/anie.200603093.

[59] M.J. Knight, A.J. Pell, I. Bertini, I.C. Felli, L. Gonnelli, R. Pierattelli, T. Hermann, L. Emsley, G. Pintacuda, Structure and backbone dynamics of a microcrystalline metalloprotein by solid-state NMR, Proc.Natl.Acad.Sci.USA. 109 (2012) 11095–11100.

[60] M.J. Knight, A.L. Webber, A.J. Pell, P. Guerry, E. Barbet-Massin, I. Bertini, I.C. Felli, L. Gonnelli, R. Pierattelli, L. Emsley, A. Lesage, T. Hermann, G. Pintacuda, Fast resonance assignment and fold determination of human superoxide dismutase by high-resolution proton-detected solid state MAS NMR spectroscopy, Angew.Chem.Int.Ed. 50 (2011) 11697–11701.

[61] P.S. Nadaud, J.J. Helmus, S.L. Kall, C.P. Jaroniec, Paramagnetic Ions Enable Tuning of Nuclear Relaxation Rates and Provide Long-Range Structural Restraints in Solid-State NMR of Proteins, J. Am. Chem. Soc. 131 (2009) 8108–8120. doi:10.1021/ja900224z.

[62] Y. Su, F. Hu, M. Hong, Paramagnetic Cu(II) For Probing Membrane Protein Structure and Function: Inhibition Mechanism of the Influenza M2 Proton Channel, J. Am. Chem. Soc. 134 (2012) 8693–8702. doi:10.1021/ja3026328.

[63] S. Parthasarathy, F. Long, Y. Miller, Y. Xiao, D. McElheny, K. Thurber, B. Ma, R. Nussinov, Y. Ishii, Molecular-Level Examination of Cu2+ Binding Structure for Amyloid Fibrils of 40-Residue Alzheimer's ? by Solid-State NMR Spectroscopy, J. Am. Chem. Soc. 133 (2011) 3390–3400. doi:10.1021/ja1072178.

[64] N.P. Wickramasinghe, S. Parthasarathy, C.R. Jones, C. Bhardwaj, F. Long, M. Kotecha, S. Mehboob, L.W.-M. Fung, J. Past, A. Samoson, Y. Ishii, Nanomole-scale Protein Solid-state NMR by Breaking Intrinsic 1H-T1 Boundaries, Nat. Methods. 6 (2009) 215–218. doi:10.1038/nmeth.1300.

[65] S. Parthasarathy, Y. Nishiyama, Y. Ishii, Sensitivity and Resolution Enhanced Solid-State NMR for Paramagnetic Systems and Biomolecules under Very Fast Magic Angle Spinning, Acc. Chem. Res. 46 (2013) 2127–2135. doi:10.1021/ar4000482.

[66] I. Sengupta, M. Gao, R.J. Arachchige, P.S. Nadaud, T.F. Cunningham, S. Saxena, C.D. Schwieters, C.P. Jaroniec, Protein structural studies by paramagnetic solid-state NMR spectroscopy aided by a compact cyclen-type Cu(II) binding tag, J. Biomol. NMR. 61 (2015) 1–6. doi:10.1007/s10858-014-9880-9.

[67] S.J. Ullrich, S. Hölper, C. Glaubitz, Paramagnetic doping of a 7TM membrane protein in lipid bilayers by Gd3+-complexes for solid-state NMR spectroscopy, J. Biomol. NMR. 58 (2014) 27–35. doi:10.1007/s10858-013-9800-4.

[68] M. Tang, D.A. Berthold, C.M. Rienstra, Solid-State NMR of a Large Membrane Protein by Paramagnetic Relaxation Enhancement, J. Phys. Chem. Lett. 2 (2011) 1836–1841. doi:10.1021/jz200768r.

[69] S. Sun, S. Yan, C. Guo, M. Li, J.C. Hoch, J.C. Williams, T. Polenova, A Timesaving Strategy for MAS NMR Spectroscopy by Combining Non-Uniform Sampling and Paramagnetic Relaxation Assisted Condensed Data Collection, J. Phys. Chem. B. 116 (2012) 13585–13596. doi:10.1021/jp3005794.

[70] L. Cerofolini, T. Staderini, S. Giuntini, E. Ravera, M. Fragai, G. Parigi, R. Pierattelli, C. Luchinat, Long-range paramagnetic NMR data can provide a closer look on metal coordination in metalloproteins, JBIC J. Biol. Inorg. Chem. 23 (2018) 71–80. doi:10.1007/s00775-017-1511-y.

[71] S. Balayssac, I. Bertini, M. Lelli, C. Luchinat, M. Maletta, K.J. Yeo, Paramagnetic ions provide precious structural restraints in solid-state NMR of proteins, J. Am. Chem. Soc. 129 (2007) 2218–2219.

[72] I. Bertini, A. Bhaumik, G. De Paepe, R.G. Griffin, M. Lelli, J.R. Lewandowski, C. Luchinat, High-Resolution Solid-State NMR Structure of a 17.6 kDa Protein, J. Am. Chem. Soc. 132 (2010) 1032–1040.

[73] I. Bertini, L. Emsley, M. Lelli, C. Luchinat, J. Mao, G. Pintacuda, Ultrafast MAS Solid-State NMR Permits Extensive 13C and 1H Detection in Paramagnetic Metalloproteins, J. Am. Chem. Soc. 132 (2010) 5558–5559. doi:10.1021/ja100398q.

[74] P. Middleton, D.P.E. Dickson, C.E. Johnson, J.D. Rush, Interpretation of the Mössbauer Spectra of the High-Potential Iron Protein from Chromatium, Eur. J. Biochem. 104 (1980) 289–296. doi:10.1111/j.1432-1033.1980.tb04427.x.

[75] I. Bertini, S. Ciurli, C. Luchinat, The electronic structure of FeS centers in proteins and models. A contribution to the understanding of their electron transfer properties., Struct.Bonding. 83 (1995) 1–54.

[76] I. Bertini, A.P. Campos, C. Luchinat, M. Teixeira, A M?ssbauer investigation of oxidized Fe_4_S_4_ HiPIP II from _Ectothiorhodospira halophila_, J.Inorg.Biochem. 52 (1993) 227–234.

[77] V. Papaefthymiou, J.J. Girerd, I. Moura, J.J.G. Moura, E. Muenck, Moessbauer study of D. gigas ferredoxin II and spin-coupling model for Fe3S4 cluster with valence delocalization, J. Am. Chem. Soc. 109 (1987) 4703–4710. doi:10.1021/ja00249a037.

[78] E. Ravera, T. Schubeis, T. Martelli, M. Fragai, G. Parigi, C. Luchinat, NMR of sedimented, fibrillized, silica-entrapped and microcrystalline (metallo) proteins, J. Magn. Reson. 253 (2015) 60–70.

[79] A. Bertarello, T. Schubeis, C. Fuccio, E. Ravera, M. Fragai, G. Parigi, L. Emsely, G. Pintacuda, C. Luchinat, Paramagnetic Properties of a Crystalline Iron-Sulfur Protein by Magic-Angle Spinning NMR Spectroscopy, Inorg. Chem. (n.d.).

[80] N.M. Loening, M. Bjerring, N.C. Nielsen, H. Oschkinat, A comparison of NCO and NCA transfer methods for biological solid-state NMR spectroscopy, J. Magn. Reson. 214 (2012) 81–90.

[81] D.H. Zhou, G. Shah, M. Cormos, C. Mullen, D. Sandoz, C.M. Rienstra, Proton-detected solid-state NMR spectroscopy of fully protonated proteins at 40 kHz magic-angle spinning, J. Am. Chem. Soc. 129 (2007) 11791–11801. doi:10.1021/ja073462m.

[82] G. Kervern, S. Steuernagel, F. Engelke, G. Pintacuda, L. Emsley, Absence of Curie relaxation in paramagnetic solids yields long ^1H coherence lifetimes, J. Am. Chem. Soc. 129 (2007) 14118–14119.

[83] I. Bertini, C. Luchinat, A. Scozzafava, Carbonic anhydrase: an insight into the zinc binding site and into the active cavity through metal substitution, Struct.Bonding. 48 (1982) 45–92.

[84] J.M. Moratal, M.-J. Martínez-Ferrer, A. Donaire, J. Castells, J. Salgado, H.R. Jiménez, Spectroscopic studies of nickel(II) carbonic anhydrase and its adducts with inorganic anions, J. Chem. Soc. Dalton Trans. 0 (1991) 3393–3399. doi:10.1039/DT9910003393.

[85] J.M. Moratal, H.R. Jiménez, J. Castells, J. Salgado, M.-J. Martínez-Ferrer, A. Donaire, 1H NMR and UV-vis spectroscopic characterization of sulfonamide complexes of nickek(II)-carbonic anhydrase. Resonance assignments based on NOE effects, J. Inorg. Biochem. 45 (1992) 231–243. doi:10.1016/0162-0134(92)84012-C.

[86] B.J. Goodfellow, I.C.N. Duarte, A.L. Macedo, B.F. Volkman, S.G. Nunes, I. Moura, J.L. Markley, J.J.G. Moura, An NMR structural study of nickel-substituted rubredoxin, JBIC J. Biol. Inorg. Chem. 15 (2010) 409–420. doi:10.1007/s00775-009-0613-6.

[87] M.R. Jensen, J.J. Led, Metal−Protein Interactions: Structure Information from Ni^{2+} -Induced Pseudocontact Shifts in a Native Nonmetalloprotein †, Biochemistry. 45 (2006) 8782–8787. doi:10.1021/bi0604431.

[88] G. Otting, Prospects for lanthanides in structural biology by NMR, J. Biomol. NMR. 42 (2008) 1–9. doi:10.1007/s10858-008-9256-0.

[89] N.C. George, J. Brgoch, A.J. Pell, C. Cozzan, A. Jaffe, G. Dantelle, A. Llobet, G. Pintacuda, R. Seshadri, B.F. Chmelka, Correlating Local Compositions and Structures with the Macroscopic Optical Properties of Ce3+-Doped CaSc2O4, an Efficient Green-Emitting Phosphor, Chem. Mater. 29 (2017) 3538–3546. doi:10.1021/acs.chemmater.6b05394.

[90] J. Li, K.B. Pilla, Q. Li, Z. Zhang, X. Su, T. Huber, J. Yang, Magic Angle Spinning NMR Structure Determination of Proteins from Pseudocontact Shifts, J. Am. Chem. Soc. 135 (2013) 8294–8303. doi:10.1021/ja4021149.

[91] A. Formanuik, A.-M. Ariciu, F. Ortu, R. Beekmeyer, A. Kerridge, F. Tuna, E.J.L. McInnes, D.P. Mills, Actinide covalency measured by pulsed electron paramagnetic resonance spectroscopy, Nat. Chem. 9 (2017) 578–583. doi:10.1038/nchem.2692.

[92] A. Bencini, I. Bertini, G. Canti, D. Gatteschi, C. Luchinat, The EPR spectra of the inhibitor derivatives of cobalt carbonic anhydrase, J.Inorg.Biochem. 14 (1981) 81–93.

[93] L. Banci, L.B. Dugad, G.N. La Mar, K.A. Keating, C. Luchinat, R. Pierattelli, _1_H Nuclear Magnetic Resonance investigation of cobalt(II) substituted carbonic anhydrase, Biophys.J. 63 (1992) 530–543.

[94] A. Schuetz, C. Wasmer, B. Habenstein, R. Verel, J. Greenwald, R. Riek, A. Böckmann, B.H. Meier, Protocols for the Sequential Solid-State NMR Spectroscopic Assignment of a Uniformly Labeled 25 kDa Protein: HET-s(1-227), ChemBioChem. 11 (2010) 1543–1551. doi:10.1002/cbic.201000124.

[95] R.S. Thakur, N.D. Kurur, P.K. Madhu, Swept-frequency two-pulse phase modulation for heteronuclear dipolar decoupling in solid-state NMR, Chem. Phys. Lett. 426 (2006) 459–463. doi:10.1016/j.cplett.2006.06.007.

[96] S. Laage, J. Sachleben, S. Steuernagel, R. Pierattelli, G. Pintacuda, L. Emsley, Fast acquisition of multi-dimensional spectra in solid-state NMR enabled by ultra-fast MAS., J.Magn.Reson. 196 (2008) 133–141.

[97] M. Fragai, C. Luchinat, G. Parigi, E. Ravera, Practical considerations over spectral quality in solid state NMR spectroscopy of soluble proteins, J. Biomol. NMR. 57 (2013) 155–166. doi:10.1007/s10858-013-9776-0.

[98] A. Mandal, J.C. Boatz, T.B. Wheeler, P.C.A. van der Wel, On the use of ultracentrifugal devices for routine sample preparation in biomolecular magic-angle-spinning NMR, J. Biomol. NMR. 67 (2017) 165–178. doi:10.1007/s10858-017-0089-6.